Published in final edited form as:
Neurobiol Dis. 2012 August ; 47(2): 280–293. doi:10.1016/j.nbd.2012.04.012.

K^+ Channel Alterations in the Progression of Experimental Autoimmune Encephalomyelitis

Peter Jukkola[1], **Amy E. Lovett-Racke**[3], **Scott S. Zamvil**[4], and **Chen Gu, Ph.D.**[1,2,*]

[1] Integrated Biomedical Graduate Program, The Ohio State University, Columbus, OH 43210

[2] Department of Neuroscience, The Ohio State University, Columbus, OH 43210

[3] Department of Microbial Infection and Immunity, The Ohio State University, Columbus, OH 43210

[4] Department of Neurology, University of California, San Francisco, San Francisco, CA 94143

Abstract

Voltage-gated K^+ (Kv) channels play critical roles not only in regulating synaptic transmission and intrinsic excitability of neurons, but also in controlling the function and proliferation of other cells in the central nervous system (CNS). The non-specific Kv channel blocker, 4-AminoPyridine (4-AP) (Dalfampridine, Ampyra®), is currently used to treat multiple sclerosis (MS), an inflammatory demyelinating disease. However, little is known how various types of Kv channels are altered in any inflammatory demyelinating diseases. By using established animal models for MS, Experimental Autoimmune Encephalomyelitis (EAE), we report that expression and distribution patterns of Kv channels are altered in the CNS correlating with EAE severity. The juxtaparanodal (JXP) targeting of Kv1.2/Kvβ2 along myelinated axons is disrupted within demyelinated lesions in the white matter of spinal cord in EAE. Moreover, somatodendritic Kv2.1 channels in the motor neurons of lower spinal cord significantly decrease correlating with EAE severity. Interestingly, Kv1.4 expression surrounding lesions is markedly up-regulated in the initial acute phase of both EAE models. Its expression in glial fibrillary acidic protein (GFAP)-positive astrocytes further increases in the remitting phase of remitting-relapsing EAE (rrEAE), but decreases in late chronic EAE (chEAE) and the relapse of rrEAE, suggesting that Kv1.4-positive astrocytes may be neuroprotective. Taken together, our studies reveal myelin-dependent and -independent alterations of Kv channels in the progression of EAE and lay a solid foundation for future study in search of a better treatment for MS.

Keywords

voltage-gated potassium (Kv) channel; experimental autoimmune encephalomyelitis (EAE); 4-AminoPyridine (4-AP); myelin; astrocyte; spinal cord

* To whom correspondence should be addressed: Chen Gu, Ph.D. 182 Rightmire Hall 1060 Carmack Road The Ohio State University Columbus, OH 43210 Phone: 614-292-0349 Fax: 614-292-5379 gu.49@osu.edu.

Introduction

MS is an inflammatory demyelinating disease of the CNS that is thought to have an autoimmune pathogenesis. Myelin damage can impair action potential (AP) propagation along axons, leading to various neurophysiological abnormalities. Ion channels are implicated in neuronal dysfunction in MS, such as axon conduction failure and axonal degeneration (Waxman, 1982; Kornek et al., 2001; Waxman, 2002; Judge and Bever, 2006; Waxman, 2006). In particular, axonal Kv channels, to hyperpolarize membrane potentials towards the resting level, play critical roles in regulating the initiation, waveform, frequency and uni-directional propagation of APs (Hodgkin and Huxley, 1952; Hille, 2001; Debanne, 2004; Gu and Barry, 2011). Blocking axonal Kv channel activity can enhance axon conduction, which may underlie the beneficial effects of 4-AP in symptomatic treatment of MS, such as improving balance, vision, walking speed and leg strength, etc (Hayes, 2004; Judge and Bever, 2006; Goodman et al., 2009; Espejo and Montalban, 2012; Goodman et al., 2010). However, the treatment does not cure MS and has side effects. This appears consistent with complex expression and targeting patterns of Kv channels.

Kv1 channels are a major subfamily of axonal Kv channels present in both the CNS and peripheral nervous system (PNS). Kv1.1, Kv1.2, and Kvβ2 are clustered in the JXP regions under the myelin sheath along myelinated axons in brain and spinal cord (Wang et al., 1993; Rhodes et al., 1995; Wang et al., 1995; Rhodes et al., 1997; Rasband et al., 1999; Vabnick et al., 1999; Rasband and Shrager, 2000; Trimmer and Rhodes, 2004). These channels constrain repetitive firing of APs in normal myelinated axons (Zhou et al., 1998), and reduce axonal excitability in pre-myelinated axons during early development and demyelinated axons in diseases (Rasband et al., 1998; Sinha et al., 2006). Furthermore, they are also present in unmyelinated axons, such as cerebellar basket cell terminals (Wang et al., 1994; Rhodes et al., 1997). Kv1.4, carrying transient currents, resides in unmyelinated hippocampal mossy fibers and in small diameter and unmyelinated axons of dorsal root ganglion neurons, but not in the JXP regions of large diameter and myelinated axons (Sheng et al., 1992; Cooper et al., 1998; Rasband et al., 2001). In contrast to axonal Kv1 channels, Kv2 channels are mainly localized in the somatodendritic regions of projection neurons, such as cortical pyramidal neurons and spinal cord motor neurons (Lim et al., 2000; Muennich and Fyffe, 2004), and therefore their targeting should not be regulated by myelin.

EAE is widely used as an animal model of human CNS demyelinating diseases, including MS. Although EAE and MS are different diseases, they share many aspects in disease pathogenic processes and EAE has been used as a model to successfully develop several effective treatments for MS (Lublin et al., 1987; Zamvil and Steinman, 1990; Steinman, 2005; Slavin et al., 2010). The chEAE and rrEAE models are induced with different myelin peptides in different mouse strains to mimic the progressive and remitting-relapsing types of MS, respectively (Youssef et al., 2002). Therefore, EAE is a good model to determine the role of Kv channels in the progression of inflammatory demyelination. In particular, the changes at the remitting stage may provide important clues for neuronal survival and remyelination.

In this study, we systematically examined the expression and targeting patterns of several key Kv channels in the CNS during the progression of chEAE and rrEAE. Our results demonstrate that they are differentially altered in various CNS cell types during EAE progression, and hence provide important insights regarding effects of Kv channel blockers on immune-mediated demyelination.

Materials and Methods

Reagents and Antibodies

The nuclear dye (Hoechst 33342) and the lipophilic dyes (Fluoromyelin-green and Fluoromyelin-red) were purchased from Invitrogen (Carlsbad, CA, USA). The following antibodies were used in our study, rabbit polyclonal anti-Kv1.2, anti-Kvβ2, anti-Kv1.4, and anti-Kv2.1 antibodies (Alomone Labs, Jerusalem, Israel), anti-Kv1.2 and anti-contactin associated protein 2 (Caspr2) antibodies (Millipore, Billerica, MA, USA), and anti-neurofilament 200 antibody (Sigma, , St Louis, MO, USA), mouse monoclonal anti-Kv1.2, anti-Kvβ2, and anti-Kv1.4 antibodies (clone #: K14/16, K17/70, and K13/31, respectively; UC Davis/NIH Neuromab Facility, Davis, CA, USA), anti-β-tubulin (Millipore), rat monoclonal anti-myelin basic protein (MBP) antibody (Chemicon, Temecula, CA, USA), goat polyclonal anti-GFAP and anti-NG2 antibodies (AbCAM, Cambridge, MA, USA), and Dylight 488-, Dylight 649-, Cy3-, and Cy5-conjugated secondary antibodies (Jackson ImmunoResearch Laboratories, West Grove, PA, USA). Myelin oligodendrocyte glycoprotein (MOG) peptide 35-55 (MEVGWYRSPFSRVVHLYRNGK) was purchased from Pro-Spec (Rehovot, Israel), and proteolipoprotein (PLP) peptide 139-151 (HCLGKWLGHPDKF) from Anaspec (Fremont, CA, USA).

Induction of chronic EAE

Complete Freund's Adjuvant (CFA) was prepared by adding ground inactivated mycobacteria tuberculosis H37Ra (Difco Laboratories, Detroit, MI, USA) to Incomplete Freund's Adjuvant (Difco Laboratories) at 4 mg/mL. CFA was passed through a glass syringe with an equal volume of sterile-filtered PBS (control) or PBS containing myelin oligodendrocyte glycoprotein (MOG) peptide 35-55 (1 mg/mL final concentration). 12-week-old female C57BL/6J mice (Jackson Laboratories, Bar Harbor, ME, USA) were immunized with 100 μL of MOG/CFA or CFA only (control) by subcutaneous injection at four sites in the belly and in each hind footpad. Pertussis toxin was injected at 0 and 2 days post immunization (DPI). Thy1:YFP transgenic mice (Jackson Laboratories) were maintained on a C57BL/6 background, and thus were immunized with the same protocol. Control mice received the same injection of CFA/PBS without the peptide. The chEAE experiment was performed 5 times, 10-17 mice per experiment. Clinical scores were assigned on a scale of 0-6 [0 = no symptoms, 1 = loss of tail tone, 2 = hindlimb paresis, 3 = moderate paralysis, 4 = paraplegia (complete hindlimb paralysis), 5 = quadriplegia, 6 = death or moribund state]. Grade 6 animals were removed from the study.

Induction of remitting-relapsing EAE

Solution preparation and immunization of 12-week-old female SJL/J mice (Jackson Laboratories) for rrEAE were performed identically to the chEAE procedures except for the use of PLP peptide 139-151. Control mice received the same injection of CFA/PBS without the peptide. The rrEAE experiment was performed 3 times, 12-15 mice per experiment.

Cardiac perfusion and tissue fixation

Animals were deeply anesthetized with 250 mg/kg avertin (12.5 mg/mL 2,2,2-tribromoethanol dissolved in ddH_20/0.025% 2-methyl-2butanol) (Sigma). The thoracic cavity was opened to expose the heart, and the mice were perfused with 20-30 mL ice-cold PBS followed by 20 mL 4% formaldehyde in PBS. The brain and spinal cord were carefully removed and post-fixed overnight in 4% formaldehyde in PBS. The brain was cut into 3-mm blocks using an acrylic brain matrix (Braintree Scientific, Braintree, MA, USA) and placed in 30% sucrose for at least 24 hr before sectioning.

Sectioning of brain and spinal cord

Brain and spinal cord tissues were arranged in the same block, embedded in optimal cutting temperature (OCT) media (Sakura Finetek USA, Inc., Torrance, CA, USA), and stored at -80 °C until sectioning. The spinal cord was cut into segments and arranged for both transverse and longitudinal sectioning. The tissue blocks were cut with a Microm HM550 cryostat (Thermo Scientific, Waltham, MA, USA) and the 40-μm sections were collected on Superfrost Plus microscope slides (FisherScientific, Pittsburgh, PA, USA) for storage at -20°C.

Immunofluorescent staining

Sections were incubated in PBS/0.2% Triton X-100 for 1 hr at room temperature to permeabilize the tissue, then blocked with 2.5% normal goat or donkey serum (matched with the host species of the secondary antibody) for 1 hr at room temperature. The primary antibodies were then added in blocking solution, and the sections were incubated for 3 hr at room temperature, then overnight at 4°C. The next day, the sections were rinsed 10 × 5 min at RT, the appropriate secondary antibody was added in blocking solution, and the sections were incubated for 3 hr at RT. Then, the sections were incubated in Hoechst 33342 and/or Fluoromyelin for 10 min at RT. Sections were rinsed 10 × 5 min at RT and coverslipped using tris-buffered Fluoro-Gel mounting media (Electron Microscopy Sciences, Hatfield, PA, USA).

Fluorescence light microscope and image capture

Fluorescence images were captured with a Spot CCD camera RT slider (Diagnostic Instruments, Sterling Heights, MI, USA) in a Zeiss upright microscope, Axiophot, using Plan Apo objectives, 2.5×/0.075, 10×/0.30, and 20×/0.50, saved as 16-bit TIFF files, and analyzed with MetaMorph (Molecular Devices, Downingtown, PA, USA) and Sigmaplot 11.0 (Systat Software, Inc., Chicago, IL, USA) for fluorescence intensity quantification. Exposure times were controlled so that the pixel intensities in the tissues of interest were below saturation, and the same exposure time was used within each group of an experiment. Image brightness and contrast were adjusted using Adobe Photoshop 7.0 (Adobe Systems Incorporated, San Jose, CA, USA). All fluorescence intensity measurements were taken from the original captured images.

Areas of interest were outlined with the region measurement tool in MetaMorph by tracing the borders of the lesions as shown by Hoechst staining. The traced region was then overlaid onto the Kv channel image, and the average intensity of the region was recorded. For control images, the average intensity of the spinal cord white matter was measured. The background intensity of the slide was measured and subtracted from region measurements for each image. For measurement of cell processes, the line measurement tool was used to trace each Kv channel-stained process directly, and the average fluorescence intensity along this line was recorded. Measurements of non-lesioned white matter regions of the same image were obtained, and were subtracted from the measurements of cell processes. For motor neurons, the somatodendritic region revealed by Kv2.1 staining was outlined and the average fluorescence intensity was recorded. Gray matter background intensity was measured for each image and subtracted from the intensity of the cells. For each experimental group, the same immunostaining and imaging procedures were used so that the fluorescence intensities can be compared within the group.

Confocal microscopy

High-magnification confocal images were captured with a Leica TCS SL confocal imaging system (Leica Microsystems, Mannheim, Germany), using a 100× HCX Plan Apo CS oil

immersion objective (numerical aperture = 1.40). Multiple channels were acquired simultaneously, and the signal was averaged over six scans. Channel crosstalk was largely eliminated through optimization of the laser line intensity by acousto-optical tunable excitation filters, and by spectral detectors allowing precisely-defined bandwidth adjustment. Images were saved as 8-bit TIFF files and adjusted for brightness and contrast using Adobe Photoshop 7.0.

Western blotting

Mice were killed with carbon dioxide, and brain and spinal cord tissues were quickly removed, flash-frozen in liquid nitrogen, and stored at -80°C until use. The tissue samples were then weighed and homogenized in 1:4 (w/v) Laemmli Sample Buffer (Bio-Rad Laboratories, Hercules, CA, USA) with 5% β-mercaptoethanol (Sigma). Protein samples were resolved by SDS-PAGE and transferred to a PVDF membrane (GE Healthcare, Piscataway, N, USA) for western blotting. The membrane was rinsed in TBST (50 mM Tris-Cl (pH 7.5), 150 mM NaCl, and 0.1% Tween20), incubated in 5% dry milk/TBST blocking solution for 1 hr at RT, and then incubated with the primary antibody in blocking solution overnight at 4°C. Membranes were then rinsed in TBST 4 × 10 min, incubated with a horseradish peroxidase-conjugated secondary antibody in blocking solution for 1 hr, and rinsed in TBST 5 × 10 min. Membranes were then incubated in ECL Plus (GE Healthcare) chemiluminescent solution for 5 min, wrapped in plastic, and exposed to X-ray film (Kodak, Rochester, NY, USA). Developed film was digitized with an Epson 3590 scanner (Epson America, Inc., Long Beach, CA, USA). The total intensities of protein bands were measured and quantified with NIH ImageJ. Background was subtracted for each band. The β-tubulin loading ratios were obtained by normalizing against the control band. The Kv channel alterations were obtained by first normalizing against their controls and further normalizing with the β-tubulin loading ratio. All Western blotting experiments were performed three times.

Hippocampal neuron culture and transfection

The hippocampal neuron culture was prepared as previously described from rat hippocampi at the embryonic day 18 (E18) (Xu et al., 2007; Barry et al., 2010; Xu et al., 2010). The neurons were transfected with cDNA constructs at 5 DIV (day *in vitro*), fixed at 7 DIV, and stained with a rabbit polyclonal anti-Kv1.4 antibody. YFP-Kv1.2 was previously described (Gu and Gu, 2011; Gu et al., 2012). YFP-Kv1.4 was made by inserting the coding sequence of yellow fluorescence protein into the N-terminal region of rat Kv1.4 between G58 and G59 with an engineered NheI site. The construct was confirmed with sequencing.

Statistical analysis

For both immunofluorescence imaging and Western blotting data, we performed One-Way ANOVA when comparing 2 or 3 experimental groups to one control group, and unpaired t-test when comparing two groups, using Sigmaplot 11.0. Results are provided as mean ± SEM.

Results

Demyelinated lesions in chEAE and rrEAE

To determine potential alterations of Kv1 channels in the pathogenic process of demyelinating diseases, chEAE was induced by immunizing C57BL/6 mice with MOG35-55, which exhibited a rapid onset and sustained clinical EAE (Fig. 1A). Since acute EAE peaked around day 20, this time point (17-20 DPI) was used to determine the initial effects of inflammation and demyelination on Kv channel expression (Fig. 1A). In addition,

day 34 was selected to determine the distribution of Kv channels in the chronic phase. SJL/J mice, immunized with PLP139-151, were used as a model of remitting-relapsing MS, the most common MS subtype. Analysis was performed on day 14 (clinical peak), 34 (remission) and 66 (relapse) to determine the changes associated with clinical signs (Fig. 1B). For immunohistochemistry studies, brains and spinal cords of EAE and control mice were dissected as shown in Fig. 1C. Coronal sections were cut from brain, and both longitudinal and cross sections were cut from spinal cord (Fig. 1C). In longitudinal sections of spinal cord, Fluoromyelin staining readily detected the areas of demyelination in the dorsal (left) and ventral (right) white matter (Fig. 1D-E). Enhanced nuclear dye staining illustrated the inflammatory cells present in the regions of myelin loss. In the remitting phase of rrEAE (25-34 DPI; showing a reduction in clinical scores by at least 2 points), both the number and the size of lesions decreased, correlating well with the EAE signs (Fig. 1E), indicating that remyelination may occur. In contrast, at the late stage of chEAE, the lesions were persistent, even somewhat increased (data not shown). Taken together, these models provide a foundation for analyzing Kv channels in the CNS at different clinical stages observed in MS patients. We asked the following questions. Do the expression and localization of Kv1 channels change during the progression of demyelinating disease, and if so, how? Do changes of channel proteins correlate with demyelination? Does Kv1 channel expression in distinct brain regions change differently during the progression? Is there any difference in Kv channel expression and localization between normal mice and those in the remitting phase of rrEAE? Are dendritic as well as axonal Kv channels altered during EAE?

Disruption of Kv1.2/Kvβ2 JXP clustering is restricted to demyelinated lesion areas in EAE

We recently determined that myelin, via a cell adhesion molecule, plays a critical role in regulating the biophysical properties as well as the JXP clustering of axonal Kv1.2 channels (Gu and Gu, 2011). Thus, demyelination observed in MS may affect axonal conduction through altering both activity and localization of these channels. We examined Kv1.2 expression and distribution in EAE. In control mice, the highly clustered pattern of Kv1.2 staining was observed in the white matter of spinal cord (Fig. 2A-C), consistent with previous reports that Kv1.2 is clustered in the JXP regions of myelinated axons (Wang et al., 1993; Rhodes et al., 1995; Vabnick et al., 1999; Rasband and Shrager, 2000). The clusters decreased or disappeared in the lesion sites for both chEAE and rrEAE (Fig. 2A,B). In some lesion sites, Kv1.2 staining appeared slightly increased, but not in clusters (Fig. 2A bottom and 2B middle). The smooth staining signals were likely contributed by Kv1.2 expression in proliferating immune cells and demyelinated axons. In some lesion sites in the rrEAE remitting phase, Kv1.2 clusters were still present, most likely resulting from partial demyelination and/or remyelination, as indicated by the reduction but not complete absence of the Fluoromyelin staining (Fig. 2B bottom). Overall, disruption of Kv1.2 clustering was highly restricted to the lesion site. In non-lesion areas, Kv1.2 clustering remained normal (Fig. 2A-C). Similar results were obtained in both chEAE and rrEAE for Kvβ2, an auxiliary subunit of Kv1 channels (Fig. 2D,E). The average fluorescence intensity of Kv1.2 remained unchanged in lesion versus non-lesion areas at different stages of both chEAE and rrEAE (Fig. 2F), indicating that there were changes in the distribution but not total amount of Kv1.2 channels. Therefore, demyelination-induced disruption of Kv1/Kvβ2 clustering is a local effect.

To determine whether Kv1.2 channel expression and distribution are altered in myelinated and unmyelinated axons, we examined other brain regions during EAE progression. In both chEAE and rrEAE, the clustering of Kv1.2 channels in unmyelinated cerebellar basket cell terminals remained unchanged (Fig. 3A), which is consistent with previous studies showing that different molecular mechanisms determine Kv1.2 clustering in different CNS regions (Ogawa et al.; 2010). However, lesions in the cerebellar white matter also disrupted Kv1.2

clustering similar to those in spinal cord white matter (data not shown). In the time frame studied, we did not observe any lesions in the corpus callosum, or any change of Kv1.2 clustering there (Fig. 3B). The overall expression levels of Kv1.2 and Kvβ2 in cerebral cortex and spinal cord remained constant at different stages of chEAE and rrEAE revealed by Western blotting, indicating there is no global alteration of these channel proteins during the progression of EAE (Fig. 3C,D), consistent with the immunostaining results (Fig. 2E).

Altered patterns of Kv1.2 targeting along axons in various lesion areas

To determine whether the reduction of Kv1.2 JXP clustering is due to the disruption of the integrity of myelinated axons in lesions, we induced chEAE in Thy1:YFP transgenic mice, which contain a subset of neurons that express YFP. Using confocal microscopy, we visualized the YFP-positive axons and Kv1.2 localization pattern. In control, Kv1.2 staining was clustered in the JXP regions of both YFP-positive and YFP-negative axons (Fig. 4A). Kv1.2 highly colocalized with a JXP marker, Caspr2 (Fig. 4A bottom). Within EAE lesions, Kv1.2 clusters markedly decreased and Kv1.2 staining was no longer restricted to the JXP regions (Fig. 4B top and Suppl. Fig. 1A). In the borderline region of a lesion, varicosities along axons were often observed, which may represent retraction bulbs of broken axons or abnormal axonal enlargements, where Kv1.2 channels were diffusely distributed (Fig. 4B bottom and Suppl. Fig. 1B). As shown by a recent study, some varicosities in the axons within lesions can recover (Nikic et al., 2011). Some axons remained myelinated in borderline regions, reflected by the presence of Kv1.2 JXP clusters (Fig. 4B bottom and Suppl. Fig. 1B).

In various lesion areas, we observed three different types of Kv1.2 alterations in the JXP clustering patterns at EAE lesions of spinal cord white matter (Fig. 4C and Suppl. Fig. 2). First, the Kv1.2 JXP cluster was elongated only on one side of the node of Ranvier, which may represent the partial or asymmetric demyelination of the axon (Fig. 4C Asymmetric). Second, the distribution of Kv1.2 became uniform over a segment of completely-demyelinated axon (Fig. 4C Uniform). Third, Kv1.2 staining became uniform but more concentrated in an axonal varicosity (Fig. 4C Varicosity). In addition to altered distribution patterns, significant reduction of Kv1.2 staining intensity along axonal segments around nodes of Ranvier was also observed during the peak stage of both chEAE (Control: 1033 ± 38 AU, n = 83; Peak: 857 ± 21 AU, n = 174; One Way ANOVA followed by Dunn's test, $p < 0.01$) and rrEAE (Control: 949 ± 30 AU, n = 167; Peak: 727 ± 20 AU, n = 149; One Way ANOVA followed by Dunn's test, $p < 0.01$) (Fig. 4C). Further reduction was observed for the chEAE late phase (Late: 603 ± 30 AU, n = 55; One Way ANOVA followed by Dunn's test, $p < 0.01$) (Fig. 4D). In sharp contrast, the staining intensity significantly recovered in the remitting phase of rrEAE (Late: 877 ± 23 AU, n = 264; One Way ANOVA followed by Dunn's test, $p > 0.05$) (Fig. 4D).

Different types of lesions were observed in this study. Based on the staining of Fluoromyelin and nuclear dye, we divided them into three major groups. The first group, type α (approximately 28% in peak chEAE; 28% in late chEAE; 17% in peak rrEAE; 10% in remitting rrEAE), includes a cyst of cells pushing axons aside without breaking them (Fig. 5). The second group, type β (approximately 62% in peak chEAE; 59% in late chEAE; 57% in peak rrEAE; 31% in remitting rrEAE), includes a dense core of cells with many broken axons failing to cross the lesion (Fig. 5). This is a major portion of lesions observed at the peak stage of both chEAE and rrEAE, which likely represent local permanent lesions in spinal cord white matter. The third group, type β (approximately 10% in peak chEAE; 14% in late chEAE; 26% in peak rrEAE; 59% in remitting rrEAE), includes lesions with less dense cell bodies and partially demyelinated areas (Fig. 5), which were more frequent in the remitting phase of rrEAE and may represent the recovering and remyelinating phase of lesions.

Somatodendritic Kv2.1 in spinal cord motor neurons during EAE progression

Alterations of axonal Kv1.2/Kvβ2 in EAE progression are largely consistent with the notion that their JXP clustering is dictated by myelin. Since in MS both motor and sensory systems are affected, we examined two other Kv channels in EAE progression, Kv2.1 expressed in the alpha motor neurons and Kv1.4 expressed in sensory neurons. In contrast to the axonal Kv1 channels, Kv2.1 channels are mainly localized in clusters in soma and proximal dendrites of spinal cord motor neurons (Lim et al., 2000; Muennich and Fyffe, 2004), and were initially used as a negative control for Kv channels in spinal cord gray matter. Surprisingly, we found a marked reduction of Kv2.1 channels in motor neurons in EAE especially in the lower spinal cord (Fig. 6A). To determine whether the reduction of Kv2.1 levels is due to neuronal cell death or channel reduction within neurons, we induced chEAE in Thy1:YFP transgenic mice. Although some reduction of YFP-positive neurons in spinal cord gray matter was observed, consistent with previous reports (Aharoni et al., 2011; Vogt et al., 2009), Kv2.1 channel levels were clearly reduced in many YFP-positive motor neurons in the lower spinal cord in chEAE (Fig. 6B). Next, we examined whether Kv2.1 levels in these motor neurons were reduced in rrEAE. Clear reduction of Kv2.1 was observed at the peak stage, similar to chEAE; yet, Kv2.1 channel levels became largely normal during the remitting phase (Fig. 6C). In upper spinal cord, the level of Kv2.1 remained unchanged in chEAE (Fig. 6D). In lower spinal cord, the level of Kv2.1 was markedly reduced in both the early and late stages of chEAE (Control: 154 ± 11.4 (AU), n = 50; Peak: 111 ± 8.6 (AU), n = 56; Late: 87 ± 4.0 (AU), n = 54) (Fig. 6E). In contrast, Kv2.1 levels were significantly reduced at the peak stage of rrEAE, but increased to normal levels in the remitting phase (Control: 138 ± 5.2 (AU), n = 67; Peak: 94 ± 4.7 (AU), n = 56; Late (remitting): 131 ± 7.0 (AU), n = 64) (Fig. 6E), correlating with clinical signs. The Kv2.1 reduction was in gray matter, and did not correlate with nearby lesion sites in white matter. Therefore, the alteration of Kv2.1 channel levels is not a consequence of demyelination.

Upregulation of Kv1.4 channels around spinal cord lesions in EAE progression

Kv1.1, Kv1.2 and Kv1.4 are the three most abundant Kv1 subunits expressed in mammalian brain. They often form heteromeric complexes predominantly in axons of some neurons, but their composition varies dramatically. The Kv1.1 subunit appears to be segregated into two major subpopulations: one associated with Kv1.2 and one associated with Kv1.4 (Vacher et al., 2008). In particular, Kv1.4 colocalizes with Kv1.1 in some unmyelinated axons of dorsal root ganglion neurons (Rasband et al., 2001). Kv1.4 expression in spinal cord white matter in adult mice is close to background (Fig. 7A,B upper panels). Surprisingly, Kv1.4 was markedly up-regulated around lesion sites in both chEAE and rrEAE at the peak stage (Fig. 7A,B middle panels). Its level declined at the late stage of chEAE, but continued to increase at the remitting stage of rrEAE (Fig. 7A,B lower panels). Interestingly, Kv1.4 was present in both round- and fiber-like structures, most likely corresponding to the cell bodies and processes of one or multiple types of cells (Fig. 7A,B).

By performing co-staining with the astrocyte marker, GFAP, we found that the processes containing up-regulated Kv1.4 were exclusively GFAP positive (Fig. 7A-D), indicating that Kv1.4 expression was specifically enhanced in astrocytes around lesions. The specificity of the rabbit polyclonal anti-Kv1.4 antibody was confirmed by robust and specific staining of cultured cells transfected with YFP-tagged Kv1.4, but not those transfected with YFP-tagged Kv1.2 (Suppl. Fig. 3). GFAP staining was clear in spinal cord white matter of control mice and increased around the lesion sites in EAE. The average fluorescence intensity of Kv1.4 in lesion and non-lesion areas in spinal cord white matter was rather consistent during the three time points in chEAE, but significantly increased in the peak and remitting phases of rrEAE. (Fig. 7E). In contrast, the Kv1.4 staining intensity along each cellular process significantly increased in both chEAE (Control: 150 ± 13 (AU), n = 162; Peak: 242 ± 10

(AU), n = 394; Late: 192 ± 8 (AU), n = 201) and rrEAE (Control: 68 ± 12 (AU), n = 45; Peak: 229 ± 12 (AU), n = 235; Late: 292 ± 11 (AU), n = 336) (Fig. 7F). This result also indicates the expression level of Kv1.4 in normal white matter is low, but not absolute zero. This is why the average level of Kv1.4 remained constant in chEAE (Fig. 7 E lef), even when its level clearly increased in astrocytic processes (Fig. 7F left). In contrast, the increase of Kv1.4 levels in rrEAE appeared to be more global (Fig. 7E right). Nonetheless, there was a clear increase of Kv1.4 levels in GFAP-positive astrocytic processes around lesion sites in both chEAE and rrEAE. Actually the number of Kv1.4-positive processes decreased in late chEAE but increased in remitting rrEAE. Importantly, we only observed Kv1.4 upregulation in fiber-like GFAP-positive astrocytes in spinal cord white matter, but never in GFAP-positive astrocytes in spinal cord gray matter (Fig. 7G,H).

Up-regulated Kv1.4 channels only partially colocalized with NG2, a marker for oligodendrocyte precursor cells, in both chEAE and rrEAE (Fig. 8A,B). NG2 staining was up-regulated around the lesion sites (Fig. 8A,B). The Kv1.4-positive processes were not NG2 positive (Fig. 8A,B). These processes were not likely axons either, as revealed in Thy1:YFP transgenic mice (Fig. 8C). No YFP-positive axon expressing Kv1.4 was ever observed (Fig. 8C). To determine the global changes of Kv1.4 in brain and spinal cord during EAE progression, we performed the Western blotting. In chEAE, there was no significant change detected at the total protein level of Kv1.4 (Fig. 8D), consistent with the immunostaining result (Fig. 7E). In rrEAE, a significant increase of Kv1.4 protein level was observed in spinal cord, but not in cortex (Fig. 8E), consistent with the immunostaining result in spinal cord (Fig. 7E). Therefore, the expression of Kv1.4 indeed appeared to increase in the spinal cord of rrEAE mice in the peak and remitting phases.

Since changes in Kv1.2, Kv2.1 and Kv1.4 correlated with severity of EAE signs in the late phase of chEAE and remitting phase of rrEAE, we wondered how these channels changed in the late relapse phase of rrEAE (Fig. 9A). At day 66, lesions were bigger and more abundant in the white matter of spinal cord and Kv1.2 JXP clustering was affected more extensively (Fig. 9B). Kv2.1 further reduced (data not shown). Importantly, the Kv1.4 levels were significantly reduced compared to the remitting phase (Kv1.4 average intensity: remitting, 292 ± 11 (AU), n = 336; relapsing, 130 ± 5 (AU), n = 279; $p < 0.01$) (Fig. 9C-E), supporting the observation that Kv channel expression is related to lesion formation and clinical signs of rrEAE. Thus, Kv channels play critical, yet diverse, roles in the functional consequences of immune-mediated demyelination.

Discussion

This is the first report of a systematical study of the expression and distribution patterns of three key Kv channels in the CNS during the progression of two types of EAEs. This study contributes to better understanding of the relationship of Kv channels to MS pathogenesis and of the therapeutic mechanism of Kv channel blockers such as 4-AP.

Localized regulation of JXP clusters of Kv1.2/Kvβ2 channels

Demyelinated lesions were present in spinal cord white matter in both chEAE and rrEAE (Fig. 1). The JXP clustering of Kv1.2/Kvβ2 was disrupted apparently only in the demyelinated lesion site (Fig. 2). In surrounding areas, they were still correctly clustered to the JXP regions. In some lesions, especially those from the remitting phase of rrEAE, Kv1.2 clusters were also present, which might be due to early or partial demyelination (Fig. 2B). However, the overall effect of demyelination on Kv1.2/Kvβ2 clustering is clear. This is consistent with the notion that myelin clusters Kv1 channels into the JXP regions. Blocking the activity of these exposed Kv channels along demyelinated axons should enhance axonal

conduction and hence potentially lead to improvement of disease symptoms of MS, which may underlie the beneficial effects of the 4-AP treatment.

In this study, we observed variations in the patterns of lesion and alteration of Kv1.2 clusters (Figs. 2-4). Lesions differed at different stages and in different EAEs. We divide them into three groups, type α, β, and γ (Fig. 5). Although their cellular and molecular identities are not the focus of the present study, they may be of interest for future investigation. Especially, in the rrEAE, how type β lesions apparently containing many broken axons in the initial exacerbation may be repaired in the remitting phase is of high interest for future studies. A recent study surprisingly shows that the varicosities forming along axons are reversible (Nikic et al., 2011), which appears to support what we have observed in this study. Moreover, completely or partially disrupted clustering patterns of Kv1.2/Kvβ2 were observed, correlating with the degree of demyelination and axonal damage (Fig. 4A-B). In the remitting phase of rrEAE, the number and size of the lesions decreased and Kv1.2 clustering recovered close to levels observed in control animals, suggesting remyelination.

We also observed weak signals from Kv1.2 channel staining in round cells within some lesions, which suggests the expression in other cell types, immune cells or glial cells, at lower levels. Kv1 channels are indeed expressed in immune/inflammatory cells (Kettenmann et al., 1993; Wulff et al., 2003a; Wulff et al., 2003b; Chandy et al., 2004; Beeton and Chandy, 2005; Farber and Kettenmann, 2005; Fordyce et al., 2005; Pannasch et al., 2006; Nutile-McMenemy et al., 2007; Wu et al., 2009). Moreover, Kv1 channel activity is required for the proliferation of oligodendrocyte precursor cells (Attali et al., 1997; Chittajallu et al., 2002), while oligodendrocyte proliferation and subsequent remyelination may be important in the remitting phase of MS. Nonetheless, neuronal dysfunction is the direct manifestation of MS.

Downregulation of Kv2.1 and upregulation of Kv1.4 during EAE progression

In this study, we surprisingly observed that Kv2.1 in motor neurons of lower spinal cord were markedly down-regulated, correlating with EAE severity (Fig. 6). At the late stage of chEAE induced in Thy1:YFP transgenic mice, YFP-positive motor neurons in spinal cord decreased, suggesting neuronal death, consistent with previous reports in MOG-induced EAE (Aharoni et al., 2011; Vogt et al., 2009). This process is most likely irreversible, consistent with sustained clinical signs in the late chEAE. In the rrEAE remitting phase, Kv2.1 staining was restored back to the normal level, suggesting that motor neuron death may not be very abundant in rrEAE, otherwise it would be difficult to understand how these motor neurons were regenerated in less than a month. Previous reports differ regarding motor neuron loss in PLP-induced EAE, showing the specific genetic background and EAE induction conditions may be important. Significant motor neuron loss was noted in adoptive transfer EAE in SJL/J mice (Vogt et al., 2009), while no loss was observed in active EAE in (SJL×Balb/c)F1 mice (Aharoni et al., 2011). Interestingly, another study shows reversible effects of EAE induced in rats on motor neuron dendritic arbors (Zhu et al., 2003), consistent with our results in rrEAE. Nonetheless, we observed many surviving motor neurons in Thy1:YFP mice. In these neurons, Kv2.1 levels were markedly reduced and its clusters were eliminated (Fig. 6B).

Kv2.1 channels form large clusters in somatodendritic regions of cortical/hippocampal pyramidal neurons and spinal cord motor neurons. Regulation of Kv2.1 clustering, extensively studied, may involve neuronal activity, protein phosphorylation, and actin cytoskeleton (O'Connell et al., 2010; Misonou et al., 2004; Misonou et al., 2006). However, the functional consequence of Kv2.1 clustering currently remains controversy (O'Connell et al., 2010; Misonou et al., 2004). In EAE, it remains unclear whether the downregulation of Kv2.1 levels and clusters is part of the pathogenic process resulting in enhanced neuronal

excitability or a compensatory mechanism to increase suppressed excitability. It will be interesting to determine whether Kv2.1 downregulation occurs in MS patients in future investigation.

In sharp contrast to the restricted alteration of Kv1.2/Kvβ2 JXP clustering (Fig. 2), the Kv2.1 downregulation did not correlate with a nearby lesion (Fig. 6). The Kv1.4 upregulation occurred not only within lesion areas, but also in the surrounding areas (Fig. 7). Therefore, diffusible factor(s) may be involved in regulating Kv2.1 and Kv1.4.

Kv1.4- and GFAP-positive astrocytes around EAE lesions and their potential function

The Kv1.4-positive processes that were markedly increased surrounding EAE lesions were exclusively colocalized with GFAP (Fig. 7), a marker usually used to identify differentiated astrocytes *in vitro* and *in vivo*. This result suggests Kv1.4 is up-regulated in activated astrocytes in spinal cord white matter. Neural stem cells giving rise to neurons and oligodendrocytes can also transiently express GFAP (Doetsch et al., 1999; Seri et al., 2001; Garcia et al., 2004). A recent study shows that reactive astrocytes in EAE were derived by proliferation and phenotypic transformation of fibrous astroglia in spinal cord white matter (Guo et al., 2011). Therefore, it is most likely that Kv1.4 is up-regulated in reactive astrocytes around EAE lesions. NG2, a marker for oligodendrocyte precursor cells, was only partially colocalized with Kv1.4-positive cells (Fig. 8A,B). Our results are consistent with the upregulation of Kv1.4 channels observed in damaged white matter in the rat model of spinal cord injury (Edwards et al., 2002) and in demyelinated lesions of mouse spinal cord of MOG-induced EAE (Herrero-Herranz et al., 2007). However, these studies show that the up-regulated Kv1.4 mainly resides in OPCs and oligodendrocytes, different from our results. Importantly, in our immunofluorescence staining of EAE, mouse antibody was not used, eliminating non-specific signals from endogenous antibodies produced by mice during EAE. In the present study, the Kv1.4-positive processes were not colocalized with myelin marker FMG, nor axonal marker YFP in Thy1:YFP transgenic mice (Fig. 8C).

Kv1.4 is expressed by a subset of astrocytes surrounding EAE lesions. GFAP-positive astrocytes are abundant in spinal cord white matter of control mice, when Kv1.4 was at a level close to the background (Fig. 7A,B). Given that Kv1.4 is up-regulated continuously in the remitting phase of rrEAE, but down-regulated in the late phase of chEAE and the relapse phase of rrEAE (Figs. 7-9), these Kv1.4-positive cells may play a neuroprotective role. For example, Nav1.5 channels are present in astrocytes and important in astrocyte function (Sontheimer et al., 1994), but are inactivated in a depolarized resting membrane potential (Sontheimer and Waxman, 1992). Upregulation of Kv1.4 could provide a more negative resting potential to make these Na^+ channels operative, and thus to enhance astrocyte electrical signaling. If up-regulated Kv1.4 plays an essential role in either the proliferation or the function of these cells, blocking Kv1.4 activity may have long-term side effects, preventing the potential remitting process.

Conclusion

This study not only has demonstrated demyelination-induced disruption of Kv1.2/Kvβ2 JXP clustering, but also surprisingly has revealed down-regulated Kv2.1 in motor neuron soma and up-regulated Kv1.4 in spinal cord astrocytes correlating with EAE severity. More importantly, by comparing their changes at different stages of chEAE and rrEAE, especially the remitting stage, we provide novel insights into motor neuron damage/recovery and the potential role of Kv1.4-positive astrocytes in remyelination. Therefore, this study has laid a solid foundation for developing an effective treatment for MS symptoms via modulation of ion channel activity.

Supplementary Material

Refer to Web version on PubMed Central for supplementary material.

Acknowledgments

We thank University of California, Davis-NIH NeuroMab facility (a nonprofit supplier) for monoclonal anti-Kv channel antibodies, Drs. D. Pitt and P. Popovich for valuable comments on the manuscript, and Mr. J Barry, Drs. Y Gu and C Shrestha for technical assistance. This work was supported by a career transition fellowship award from the National Multiple Sclerosis Society (Grant TA3012A1) and a grant from National Institute of Neurological Disorders and Stroke/National Institutes of Health (R01NS062720) to C.G., by grants from the NIH (RO1 AI073737 and RO1 NS063008), NMSS (RG 4124), Guthy Jackson Charitable Foundation and Maisin Foundation to S.S.Z., and by Neuroscience Imaging Core grant P30 NS045758. All animal experiments have been conducted in accordance with the NIH Animal Use Guidelines.

References

Aharoni R, Vainshtein A, Stock A, Eilam R, From R, Shinder V, Arnon R. Distinct pathological patterns in relapsing-remitting and chronic models of experimental autoimmune enchephalomyelitis and the neuroprotective effect of glatiramer acetate. J Autoimmun. 2011; 37:228–241. [PubMed: 21752599]

Attali B, Wang N, Kolot A, Sobko A, Cherepanov V, Soliven B. Characterization of delayed rectifier Kv channels in oligodendrocytes and progenitor cells. J Neurosci. 1997; 17:8234–8245. [PubMed: 9334399]

Barry J, Gu Y, Gu C. Polarized targeting of L1-CAM regulates axonal and dendritic bundling in vitro. Eur J Neurosci. 2010; 32:1618–1631. [PubMed: 20964729]

Beeton C, Chandy KG. Potassium channels, memory T cells, and multiple sclerosis. Neuroscientist. 2005; 11:550–562. [PubMed: 16282596]

Chandy KG, Wulff H, Beeton C, Pennington M, Gutman GA, Cahalan MD. K^+ channels as targets for specific immunomodulation. Trends Pharmacol Sci. 2004; 25:280–289. [PubMed: 15120495]

Chittajallu R, Chen Y, Wang H, Yuan X, Ghiani CA, Heckman T, McBain CJ, Gallo V. Regulation of Kv1 subunit expression in oligodendrocyte progenitor cells and their role in G1/S phase progression of the cell cycle. Proc Natl Acad Sci U S A. 2002; 99:2350–2355. [PubMed: 11854528]

Cooper EC, Milroy A, Jan YN, Jan LY, Lowenstein DH. Presynaptic localization of Kv1.4-containing A-type potassium channels near excitatory synapses in the hippocampus. J Neurosci. 1998; 18:965–974. [PubMed: 9437018]

Debanne D. Information processing in the axon. Nat Rev Neurosci. 2004; 5:304–316. [PubMed: 15034555]

Doetsch F, Caille I, Lim DA, Garcia-Verdugo JM, Alvarez-Buylla A. Subventricular zone astrocytes are neural stem cells in the adult mammalian brain. Cell. 1999; 97:703–716. [PubMed: 10380923]

Edwards L, Nashmi R, Jones O, Backx P, Ackerley C, Becker L, Fehlings MG. Upregulation of Kv 1.4 protein and gene expression after chronic spinal cord injury. J Comp Neurol. 2002; 443:154–167. [PubMed: 11793353]

Espejo C, Montalban X. Dalfampridine in multiple sclerosis: From symptomatic treatment to immunomodulation. Clin Immunol. 2012; 142:84–92. [PubMed: 21742559]

Farber K, Kettenmann H. Physiology of microglial cells. Brain Res Brain Res Rev. 2005; 48:133–143. [PubMed: 15850652]

Fordyce CB, Jagasia R, Zhu X, Schlichter LC. Microglia Kv1.3 channels contribute to their ability to kill neurons. J Neurosci. 2005; 25:7139–7149. [PubMed: 16079396]

Garcia AD, Doan NB, Imura T, Bush TG, Sofroniew MV. GFAP-expressing progenitors are the principal source of constitutive neurogenesis in adult mouse forebrain. Nat Neurosci. 2004; 7:1233–1241. [PubMed: 15494728]

Goodman AD, Brown TR, Edwards KR, Krupp LB, Schapiro RT, Cohen R, Marinucci LN, Blight AR. A phase 3 trial of extended release oral dalfampridine in multiple sclerosis. Ann Neurol. 2010; 68:494–502. [PubMed: 20976768]

Goodman AD, Brown TR, Krupp LB, Schapiro RT, Schwid SR, Cohen R, Marinucci LN, Blight AR. Sustained-release oral fampridine in multiple sclerosis: a randomised, double-blind, controlled trial. Lancet. 2009; 373:732–738. [PubMed: 19249634]

Gu C, Barry J. Function and mechanism of axonal targeting of voltage-sensitive potassium channels. Prog Neurobiol. 2011; 94:115–132. [PubMed: 21530607]

Gu C, Gu Y. Clustering and activity tuning of kv1 channels in myelinated hippocampal axons. J Biol Chem. 2011; 286:25835–25847. [PubMed: 21602278]

Gu Y, Gu C. Dynamics of Kv1 channel transport in axons. PLoS One. 2010; 5:e11931. [PubMed: 20694152]

Gu Y, Barry J, McDougel R, Terman D, Gu C. Alternative splicing regulates Kv3.1 polarized targeting to adjust maximal spiking frequency. J Biol Chem. 2012; 287:1755–1769. [PubMed: 22105078]

Guo F, Maeda Y, Ma J, Delgado M, Sohn J, Miers L, Ko EM, Bannerman P, Xu J, Wang Y, Zhou C, Takebayashi H. Pleasure D Macroglial plasticity and the origins of reactive astroglia in experimental autoimmune encephalomyelitis. J Neurosci. 31:11914–11928. [PubMed: 21849552]

Hayes KC. The use of 4-aminopyridine (fampridine) in demyelinating disorders. CNS Drug Rev. 2004; 10:295–316. [PubMed: 15592580]

Herrero-Herranz E, Pardo LA, Bunt G, Gold R, Stuhmer W, Linker RA. Re-expression of a developmentally restricted potassium channel in autoimmune demyelination: Kv1.4 is implicated in oligodendroglial proliferation. Am J Pathol. 2007; 171:589–598. [PubMed: 17600124]

Hille, B. Ion channels of excitable membranes. Sinauer; Sunderland, Massachusetts: 2001. 2001

Hodgkin AL, Huxley AF. Currents carried by sodium and potassium ions through the membrane of the giant axon of Loligo. J Physiol. 1952; 116:449–472. [PubMed: 14946713]

Judge SI, Bever CT Jr. Potassium channel blockers in multiple sclerosis: neuronal Kv channels and effects of symptomatic treatment. Pharmacol Ther. 2006; 111:224–259. [PubMed: 16472864]

Kettenmann H, Banati R, Walz W. Electrophysiological behavior of microglia. Glia. 1993; 7:93–101. [PubMed: 7678582]

Kornek B, Storch MK, Bauer J, Djamshidian A, Weissert R, Wallstroem E, Stefferl A, Zimprich F, Olsson T, Linington C, Schmidbauer M, Lassmann H. Distribution of a calcium channel subunit in dystrophic axons in multiple sclerosis and experimental autoimmune encephalomyelitis. Brain. 2001; 124:1114–1124. [PubMed: 11353727]

Lim ST, Antonucci DE, Scannevin RH, Trimmer JS. A novel targeting signal for proximal clustering of the Kv2.1 K^+ channel in hippocampal neurons. Neuron. 2000; 25:385–397. [PubMed: 10719893]

Lublin FD, Lavasa M, Viti C, Knobler RL. Suppression of acute and relapsing experimental allergic encephalomyelitis with mitoxantrone. Clin Immunol Immunopathol. 1987; 45:122–128. [PubMed: 3621681]

Misonou H, Menegola M, Mohapatra DP, Guy LK, Park KS, Trimmer JS. Bidirectional activity-dependent regulation of neuronal ion channel phosphorylation. J Neurosci. 2006; 26:13505–13514. [PubMed: 17192433]

Misonou H, Mohapatra DP, Park EW, Leung V, Zhen D, Misonou K, Anderson AE, Trimmer JS. Regulation of ion channel localization and phosphorylation by neuronal activity. Nat Neurosci. 2004; 7:711–718. [PubMed: 15195093]

Muennich EA, Fyffe RE. Focal aggregation of voltage-gated, Kv2.1 subunit-containing, potassium channels at synaptic sites in rat spinal motoneurones. J Physiol. 2004; 554:673–685. [PubMed: 14608003]

Nikic I, Merkler D, Sorbara C, Brinkoetter M, Kreutzfeldt M, Bareyre FM, Bruck W, Bishop D, Misgeld T, Kerschensteiner M. A reversible form of axon damage in experimental autoimmune encephalomyelitis and multiple sclerosis. Nat Med. 2011; 17:495–499. [PubMed: 21441916]

Nutile-McMenemy N, Elfenbein A, Deleo JA. Minocycline decreases in vitro microglial motility, beta1-integrin, and Kv1.3 channel expression. J Neurochem. 2007; 103:2035–2046. [PubMed: 17868321]

O'Connell KM, Loftus R, Tamkun MM. Localization-dependent activity of the Kv2.1 delayed-rectifier K^+ channel. Proc Natl Acad Sci U S A. 107:12351–12356. [PubMed: 20566856]

Ogawa Y, Oses-Prieto J, Kim MY, Horresh I, Peles E, Burlingame AL, Trimmer JS, Meijer D, Rasband MN. ADAM22, a Kv1 channel-interacting protein, recruits membrane-associated guanylate kinases to juxtaparanodes of myelinated axons. J Neurosci. 2010; 30:1038–1048. [PubMed: 20089912]

Pannasch U, Farber K, Nolte C, Blonski M, Yan Chiu S, Messing A, Kettenmann H. The potassium channels Kv1.5 and Kv1.3 modulate distinct functions of microglia. Mol Cell Neurosci. 2006; 33:401–411. [PubMed: 17055293]

Rasband MN, Shrager P. Ion channel sequestration in central nervous system axons. J Physiol 525 Pt. 2000; 1:63–73.

Rasband MN, Trimmer JS, Peles E, Levinson SR, Shrager P. K^+ channel distribution and clustering in developing and hypomyelinated axons of the optic nerve. J Neurocytol. 1999; 28:319–331. [PubMed: 10739574]

Rasband MN, Park EW, Vanderah TW, Lai J, Porreca F, Trimmer JS. Distinct potassium channels on pain-sensing neurons. Proc Natl Acad Sci U S A. 2001; 98:13373–13378. [PubMed: 11698689]

Rasband MN, Trimmer JS, Schwarz TL, Levinson SR, Ellisman MH, Schachner M, Shrager P. Potassium channel distribution, clustering, and function in remyelinating rat axons. J Neurosci. 1998; 18:36–47. [PubMed: 9412484]

Rhodes KJ, Keilbaugh SA, Barrezueta NX, Lopez KL, Trimmer JS. Association and colocalization of K^+ channel alpha- and beta-subunit polypeptides in rat brain. J Neurosci. 1995; 15:5360–5371. [PubMed: 7623158]

Rhodes KJ, Strassle BW, Monaghan MM, BekeleArcuri Z, Matos MF, Trimmer JS. Association and colocalization of the Kv beta 1 and Kv beta 2 beta-subunits with Kv1 alpha-subunits in mammalian brain K+ channel complexes. Journal of Neuroscience. 1997; 17:8246–8258. [PubMed: 9334400]

Seri B, Garcia-Verdugo JM, McEwen BS, Alvarez-Buylla A. Astrocytes give rise to new neurons in the adult mammalian hippocampus. J Neurosci. 2001; 21:7153–7160. [PubMed: 11549726]

Sheng M, Tsaur ML, Jan YN, Jan LY. Subcellular Segregation of two A-type K^+ channel proteins in rat central neurons. Neuron. 1992; 9:271–284. [PubMed: 1497894]

Sinha K, Karimi-Abdolrezaee S, Velumian AA, Fehlings MG. Functional changes in genetically dysmyelinated spinal cord axons of shiverer mice: role of juxtaparanodal Kv1 family K^+ channels. J Neurophysiol. 2006; 95:1683–1695. [PubMed: 16319208]

Slavin A, Kelly-Modis L, Labadia M, Ryan K, Brown ML. Pathogenic mechanisms and experimental models of multiple sclerosis. Autoimmunity. 2010; 43:504–513. [PubMed: 20380590]

Sontheimer H, Waxman SG. Ion channels in spinal cord astrocytes in vitro. II. Biophysical and pharmacological analysis of two Na+ current types. J Neurophysiol. 1992; 68:1001–1011. [PubMed: 1331355]

Sontheimer H, Fernandez-Marques E, Ullrich N, Pappas CA, Waxman SG. Astrocyte Na^+ channels are required for maintenance of Na^+/K^+-ATPase activity. J Neurosci. 1994; 14:2464–2475. [PubMed: 8182422]

Steinman L. Blocking adhesion molecules as therapy for multiple sclerosis: natalizumab. Nat Rev Drug Discov. 2005; 4:510–518. [PubMed: 15931259]

Trimmer JS, Rhodes KJ. Localization of voltage-gated ion channels in mammalian brain. Annu Rev Physiol. 2004; 66:477–519. [PubMed: 14977411]

Vabnick I, Trimmer JS, Schwarz TL, Levinson SR, Risal D, Shrager P. Dynamic potassium channel distributions during axonal development prevent aberrant firing patterns. J Neurosci. 1999; 19:747–758. [PubMed: 9880595]

Vacher H, Mohapatra DP, Trimmer JS. Localization and targeting of voltage-dependent ion channels in mammalian central neurons. Physiol Rev. 2008; 88:1407–1447. [PubMed: 18923186]

Vogt J, Paul F, Aktas O, Muller-Wielsch K, Dorr J, Dorr S, Bharathi BS, Glumm R, Schmitz C, Steinbusch H, Raine CS, Tsokos M, Nitsch R, Zipp F. Lower motor neuron loss in multiple sclerosis and experimental autoimmune encephalomyelitis. Ann Neurol. 2009; 66:310–322. [PubMed: 19798635]

Wang H, Kunkel DD, Schwartzkroin PA, Tempel BL. Localization of Kv1.1 and Kv1.2, two K channel proteins, to synaptic terminals, somata, and dendrites in the mouse brain. J Neurosci. 1994; 14:4588–4599. [PubMed: 8046438]

Wang H, Kunkel DD, Martin TM, Schwartzkroin PA, Tempel BL. Heteromultimeric K^+ channels in terminal and juxtaparanodal regions of neurons. Nature. 1993; 365:75–79. [PubMed: 8361541]

Wang H, Allen ML, Grigg JJ, Noebels JL, Tempel BL. Hypomyelination alters K^+ channel expression in mouse mutants shiverer and Trembler. Neuron. 1995; 15:1337–1347. [PubMed: 8845157]

Waxman SG. Membranes, myelin, and the pathophysiology of multiple sclerosis. New England J Med. 1982; 306:1529–1533. [PubMed: 7043271]

Waxman SG. Ion channels and neuronal dysfunction in multiple sclerosis. Arch Neurol. 2002; 59:1377–1380. [PubMed: 12223023]

Waxman SG. Axonal conduction and injury in multiple sclerosis: the role of sodium channels. Nat Rev Neurosci. 2006; 7:932–941. [PubMed: 17115075]

Wu CY, Kaur C, Sivakumar V, Lu J, Ling EA. Kv1.1 expression in microglia regulates production and release of proinflammatory cytokines, endothelins and nitric oxide. Neuroscience. 2009; 158:1500–1508. [PubMed: 19118603]

Wulff H, Beeton C, Chandy KG. Potassium channels as therapeutic targets for autoimmune disorders. Curr Opin Drug Discov Devel. 2003a; 6:640–647.

Wulff H, Calabresi PA, Allie R, Yun S, Pennington M, Beeton C, Chandy KG. The voltage-gated Kv1.3 K^+ channel in effector memory T cells as new target for MS. J Clin Invest. 2003b; 111:1703–1713. [PubMed: 12782673]

Xu M, Gu Y, Barry J, Gu C. Kinesin I transports tetramerized Kv3 channels through the axon initial segment via direct binding. J Neurosci. 2010; 30:15987–16001. [PubMed: 21106837]

Xu M, Cao R, Xiao R, Zhu MX, Gu C. The axon-dendrite targeting of Kv3 (Shaw) channels is determined by a targeting motif that associates with the T1 domain and ankyrin G. J Neurosci. 2007; 27:14158–14170. [PubMed: 18094255]

Youssef S, Stuve O, Patarroyo JC, Ruiz PJ, Radosevich JL, Hur EM, Bravo M, Mitchell DJ, Sobel RA, Steinman L, Zamvil SS. The HMG-CoA reductase inhibitor, atorvastatin, promotes a Th2 bias and reverses paralysis in central nervous system autoimmune disease. Nature. 2002; 420:78–84. [PubMed: 12422218]

Zamvil SS, Steinman L. The T lymphocyte in experimental allergic encephalomyelitis. Annu Rev Immunol. 1990; 8:579–621. [PubMed: 2188675]

Zhou L, Zhang CL, Messing A, Chiu SY. Temperature-sensitive neuromuscular transmission in Kv1.1 null mice: role of potassium channels under the myelin sheath in young nerves. J Neurosci. 1998; 18:7200–7215. [PubMed: 9736643]

Zhu B, Luo L, Moore GR, Paty DW, Cynader MS. Dendritic and synaptic pathology in experimental autoimmune encephalomyelitis. American J Pathol. 2003; 162:1639–1650.

Highlights

>A non-selective blocker of Kv channels is used to treat MS symptoms.

>We examined the expression and distribution of three key Kv channels in murine EAEs.

>Redistribution of axonal Kv1.2/Kvβ2 is myelin dependent.

>Surprising Kv2.1 downregulation and Kv1.4 upregulation are myelin independent.

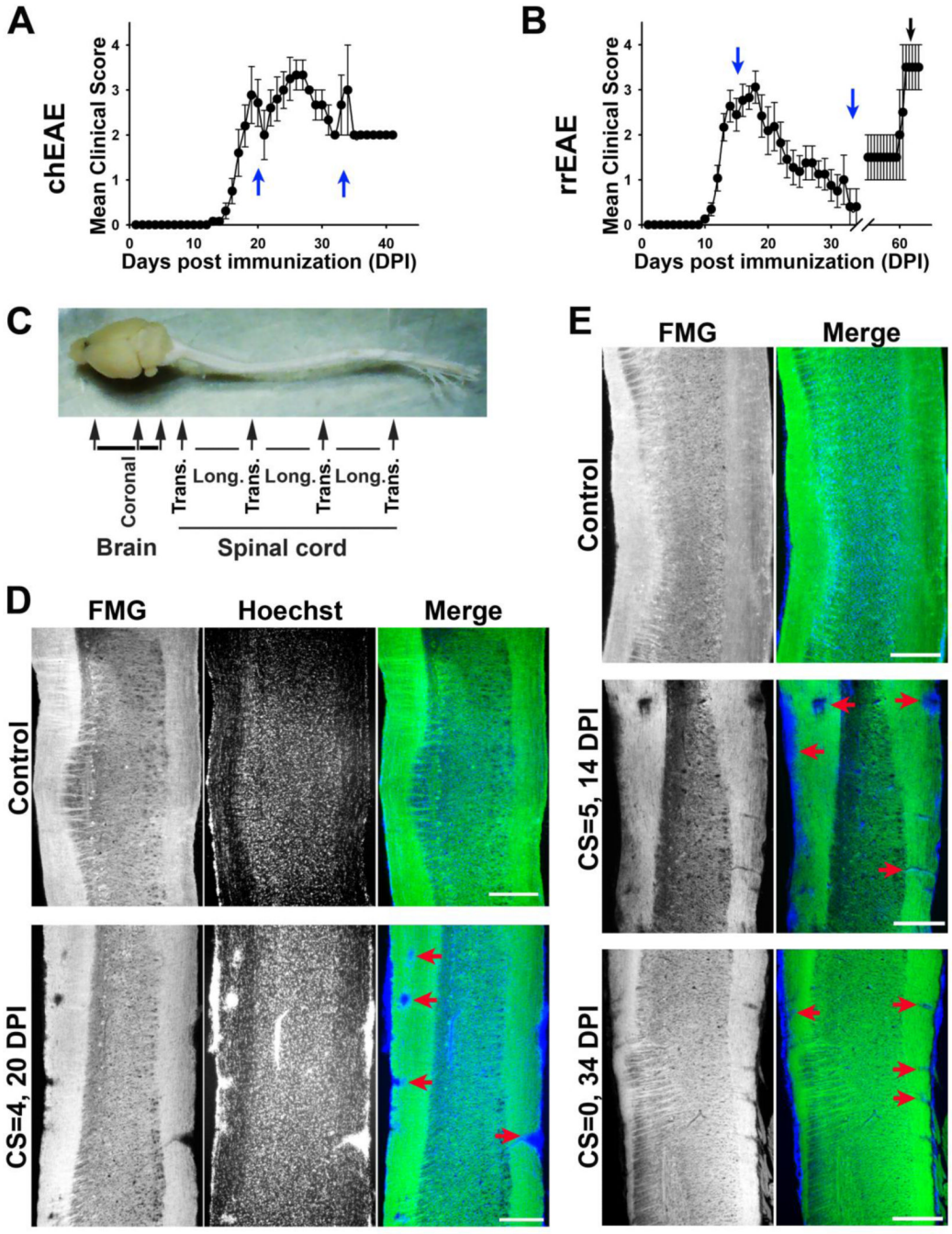

Figure 1. Lesions in the white matter of spinal cord of chEAE and rrEAE mice

(**A**) The time course of chEAE progression indicated by mean clinical scores. Female C57BL/6J mice were immunized with MOG peptide 35-55 at day 0 and monitored continuously until 41 DPI. (**B**) The time course of rrEAE progression. Female SJL/J mice were immunized with PLP peptide 139-151 at day 0 and monitored continuously until 65 DPI. Two blue arrows show the peak and late stages of EAE progression. Both chEAE and rrEAE were induced at least three times with 10-17 mice each time, producing consistent results. The black arrow shows the relapsing stage of rrEAE with fewer mice. (**C**) Sectioning of dissected mouse brain and spinal cord. Coronal sections were obtained for cerebral cortex and cerebellum. Both longitudinal and cross sections were obtained

alternatively from spinal cord. (**D**) Lesions in the white matter of chEAE spinal cord. In the longitudinal section of control spinal cord (top), the white matter on both sides were labeled with Fluoromyelin green (FMG, green in merged). Cells, more concentrated in gray matter, were labeled with a nuclear dye, Hoechst (blue in merged). In chEAE spinal cord (bottom) at 20 DPI with a clinical score (CS) of 4, multiple lesion areas (red arrows) were observed, characterized by both clusters of cells (indication of inflammation) and the absence of FMG (indication of demyelination). (**E**) Lesions in the white matter of rrEAE spinal cord. Spinal cord sections from mice of control (top), at the peak stage (middle), and at the remitting stage (bottom; Note that this mouse previously scored CS = 4 at the peak stage), are shown. Their stages (DPI) and final CSs are indicated on the left. Red arrows indicate lesions with both decreased FMG and clusters of nuclear dye staining. Scale bars, 1500 μm.

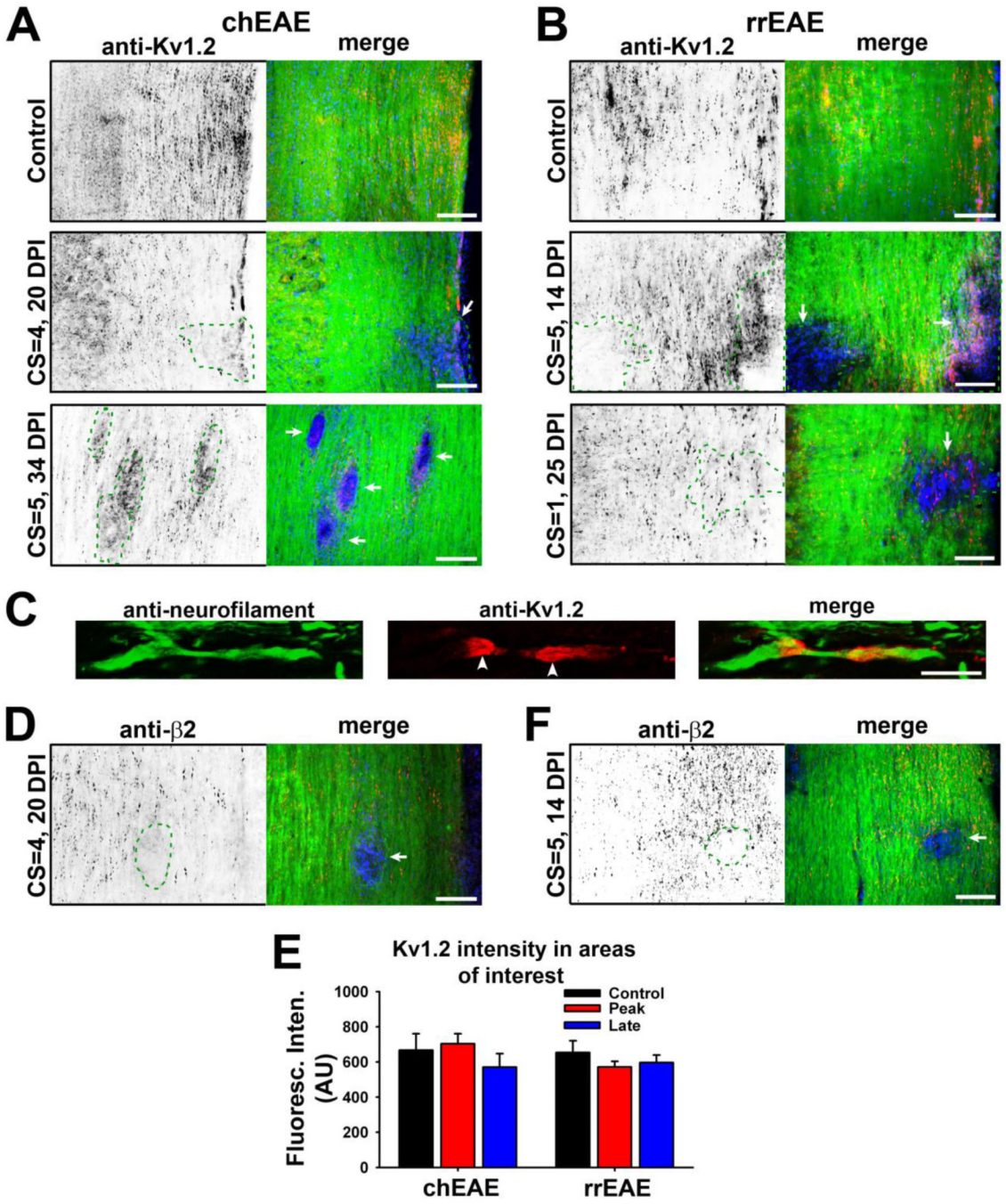

Figure 2. Alterations of Kv1.2/Kvβ2 JXP targeting within lesion areas in EAE spinal cord

(**A**) Kv1.2 JXP clustering in myelinated axons of spinal cord white matter was altered in chEAE lesions. Kv1.2 staining signals are inverted (left) and are in red in the merged image (right). In merged images, FMG staining is in green and nuclear staining in blue. Staining images from spinal cord sections of the mice of control (top), at the peak stage (middle), and at the late stage (bottom), are shown. DPI and CS of each mouse are provided on the left. (**B**) Kv1.2 JXP clustering was altered in rrEAE lesions. Shown are staining images from spinal cord sections of the mice of control (top), at the peak stage (middle), and at the remitting stage (bottom). (**C**) Confocal image of the costaining of neurofilament (green) and

Kv1.2 (red) along normal myelinated axon. White arrowheads, Kv1.2 JXP clusters. (**D**) Kvβ2 JXP clustering was disrupted in lesions of chEAE spinal cord. (**E**) Kvβ2 JXP clustering was disrupted in lesions of rrEAE spinal cord. Lesion areas are enclosed with dashed green lines and indicated with white arrows in merged images. (**F**) The expression of Kv1.2 in the areas with or without a lesion in spinal cord white matter at different stages of chEAE (left) and rrEAE (right). In chEAE, the average Kv1.2 staining intensities of spinal cord white matter are 667 ± 94 (AU, n = 18) in control areas, 703 ± 57 (AU, n = 13) in lesion areas from peak chEAE, and 571 ± 76 (AU, n = 15) in lesion areas from late chEAE. In rrEAE, the average Kv1.2 staining intensities are 653 ± 67 (AU, n = 16) in control areas, 571 ± 33 (AU, n = 15) in lesion areas from the peak stage, and 596 ± 43 (AU, n = 20) in lesion areas from the remitting stage. No significant difference was detected among the groups (One-Way ANOVA followed by Dunn's test, $p > 0.05$). Average fluorescence intensities of different areas of interest were measured, quantified, and shown as mean ± SEM. Background fluorescence intensity was subtracted. The result was obtained from at least three groups of mice. Scale bars, 200 μm in (**A**), (**B**), (**D**) and (**E**); 5 μm in (**C**).

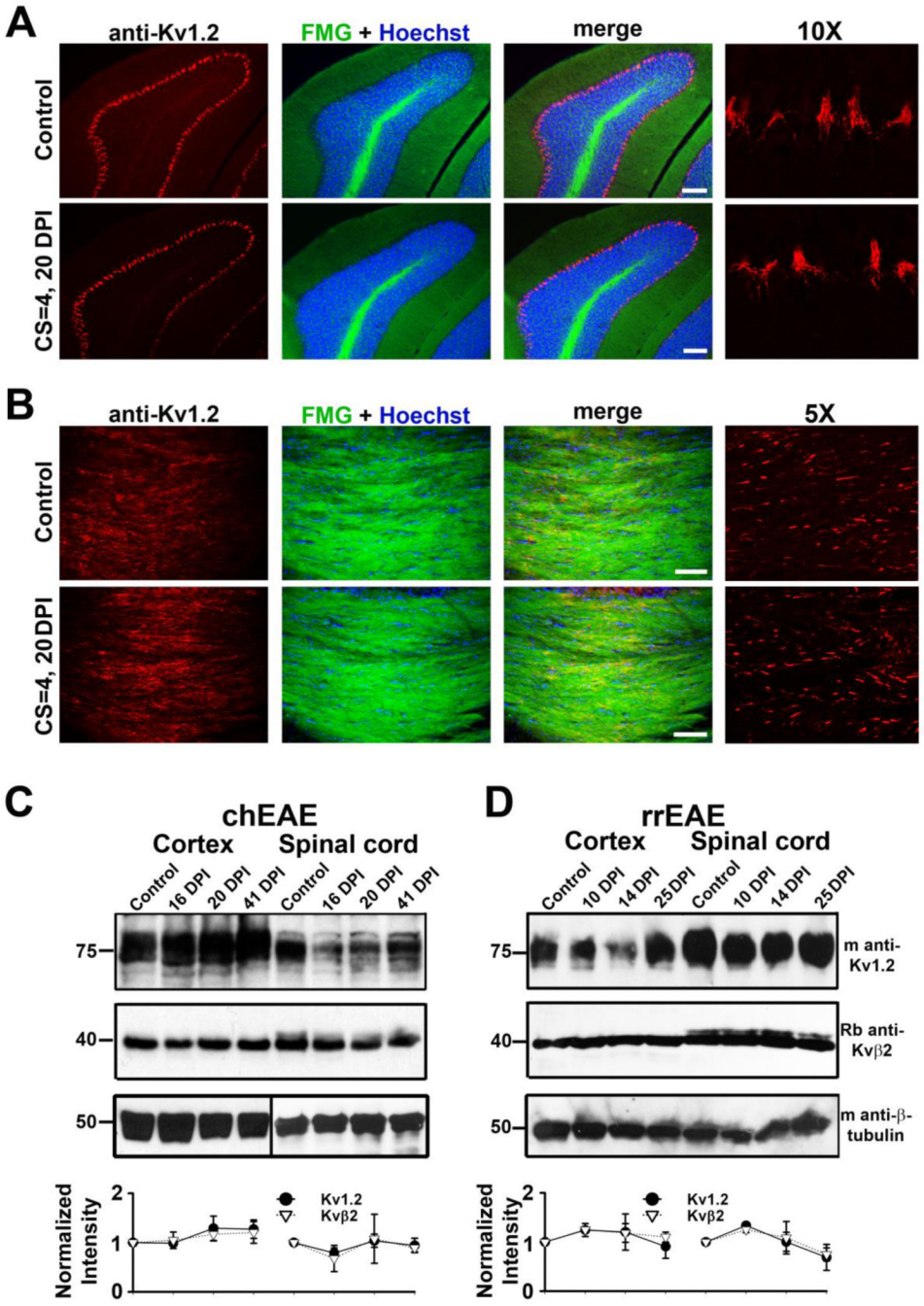

Figure 3. Kv1.2 expression patterns and levels in brain regions during EAE progression

(**A**) Kv1.2 clustering in cerebellar basket cell terminals was not affected during chEAE progression. Coronal sections of cerebellum from control (top) and chEAE (bottom) mice are shown. DPI and CS are provided on the left. Kv1.2 staining is in red, FMG in green, and Hoechst staining in blue. Images with 10-fold higher magnification showing Kv1.2 staining (red) in basket cell terminals are on the far right. (**B**) No lesion was observed in corpus callosum and no change in Kv1.2 JXP targeting. The image was from corpus callosum linking two hemispheres in a coronal section of mouse brain. Images with 5-fold higher magnification showing Kv1.2 staining (red) in JXP clusters of myelinated axons in corpus callosum are on the far right. Scale bars, 200 μm. The global expression of Kv1.2/Kvβ2 in

cerebral cortex and spinal cord at different stages of chEAE (**C**) and rrEAE (**D**) revealed by Western blotting. Molecular weights were labeled on the left in kDa. Each set of experiment contains four different time points, control, and at early peak, peak, and late stages. Equal amounts of tissue samples were loaded on the gel within each set. Mouse anti-Kv1.2 and rabbit anti-Kvβ2 antibodies were used in the Western blotting. Mouse monoclonal anti-β-tubulin was used as a control for protein loading. The intensities of protein bands were measured, normalized with the controls, further normalized with the ratio of β-tubulin staining, and provided as mean ± SEM (bottom). Background intensity was subtracted for each measurement.

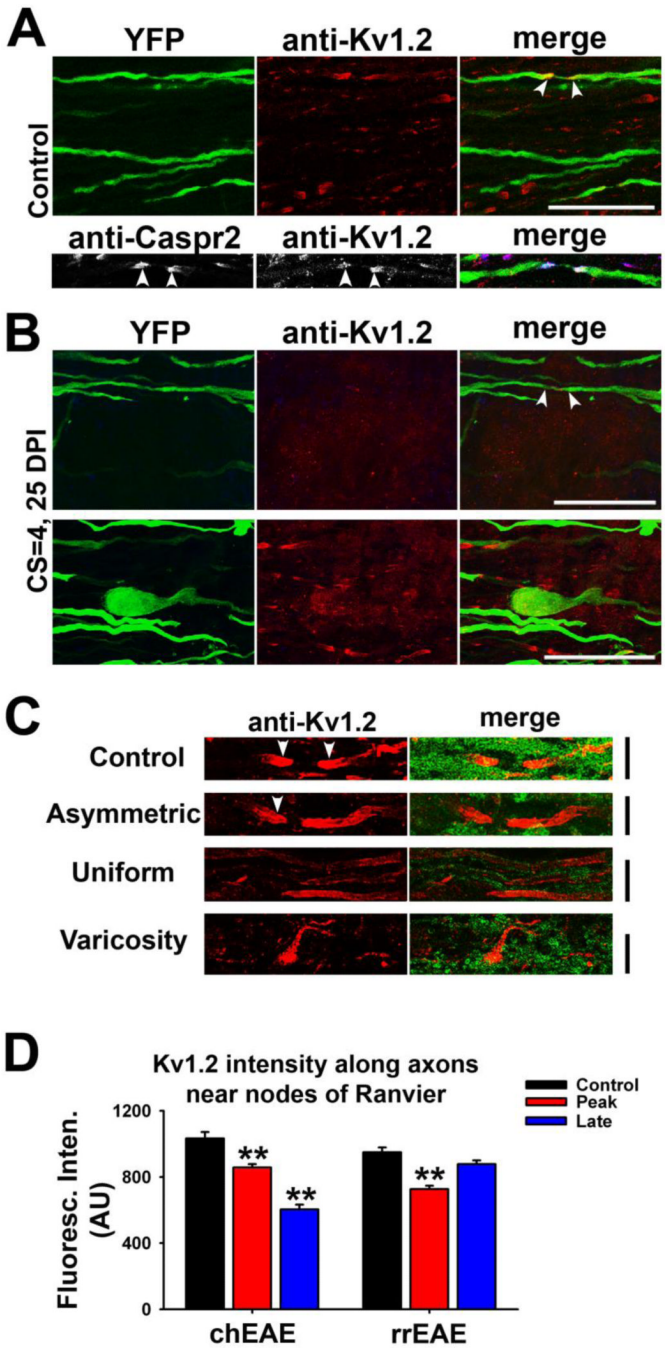

Figure 4. Alterations of Kv1.2 targeting patterns along axons within EAE lesions

(**A**) Kv1.2 JXP clustering along myelinated axons in spinal cord white matter of Thy1:YFP transgenic mouse. In upper panels, YFP-positive axons are shown in green and anti-Kv1.2 staining in red. The lower panels show Kv1.2 (red in merged) co-clustered with Caspr2 (blue in merged), a JXP marker, along a YFP-expressing axon. White arrowheads, putative JXP regions flanking nodes of Ranvier. (**B**) In upper panels, Kv1.2 JXP clusters within a chEAE lesion (see Suppl. Fig. 1A) were eliminated, while several YFP-positive axons were still present. In lower panels, this area was from the borderline of a chEAE lesion (see Suppl. Fig. 1B). A potential retraction bulb was present, whereas some Kv1.2 clusters were

present in surrounding axons. DPI and CS are provided on the left. Scale bars, 20 μm. (**C**) Different patterns of altered Kv1.2 JXP targeting in demyelinated lesions. Kv1.2 staining in red and FMG staining in green. Control, normal Kv1.2 JXP targeting in control mouse; Asymmetric, only one of the Kv1.2 JXP clusters elongated; Uniform, Kv1.2 distributed uniformly along demyelinated axons; Varicosity, Kv1.2 distribution pattern in enlarged axonal segments or retraction bulbs. Scale bars, 10 μm. (**D**) Average Kv1.2 staining intensities along axonal segments near nodes of Ranvier of axons within and outside the lesions. One-Way ANOVA followed by Dunn's test, ** $p < 0.01$.

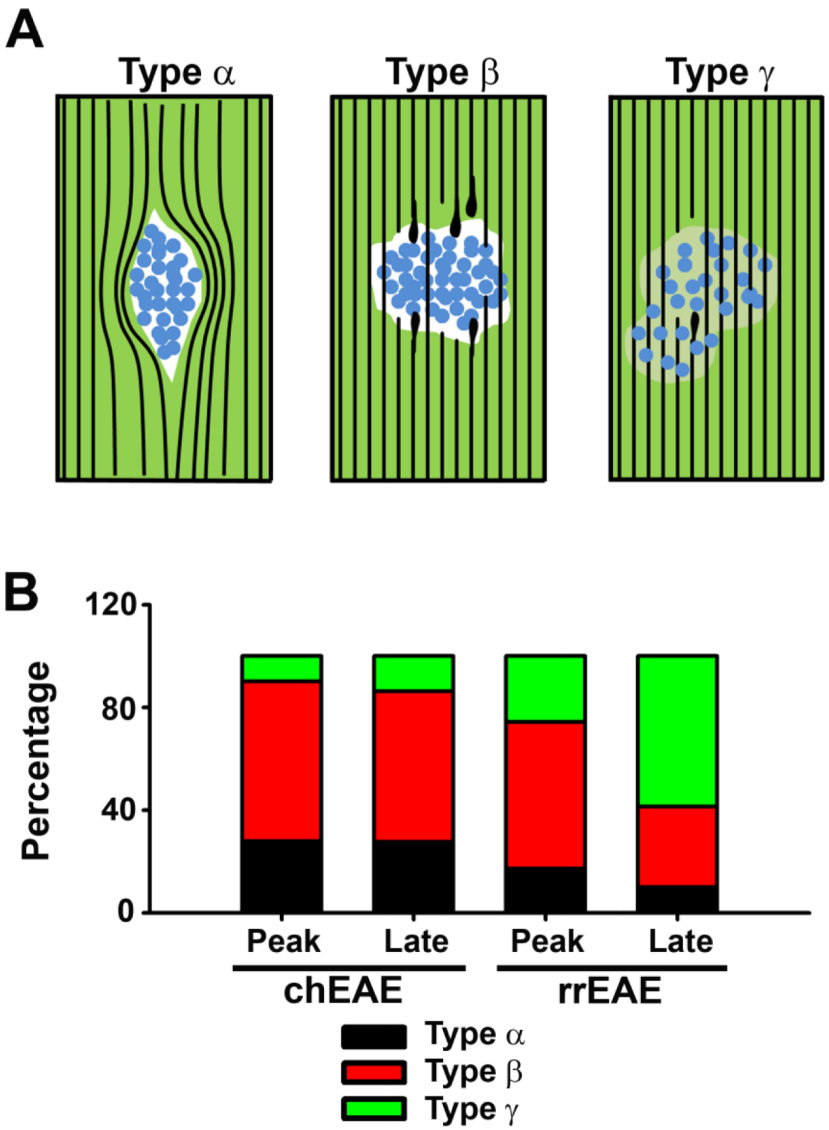

Figure 5. Different types of lesions in spinal cord white matter of chEAE and rrEAE

(**A**) Illustration of three major types (α, β and γ) of lesions observed in spinal cord white matter of chEAE and rrEAE mice. Black lines, axons revealed by Kv1.2/Kvβ2 staining and YFP fluorescence of the Thy1:YFP transgenic mice; Blue circles, proliferating cells revealed by nuclear dye (Hoechst) staining (potentially the proliferated inflammatory cells); Green areas, myelinated axons labeled with FMG; White areas, demyelination lesions with no FMG staining; Light green areas, partially demyelinated areas. (**B**) Percentage of different lesion types at the peak and late stages of chEAE (Peak: n = 61; Late: n = 58) and rrEAE (Peak: n = 70; Late (remitting): n = 70).

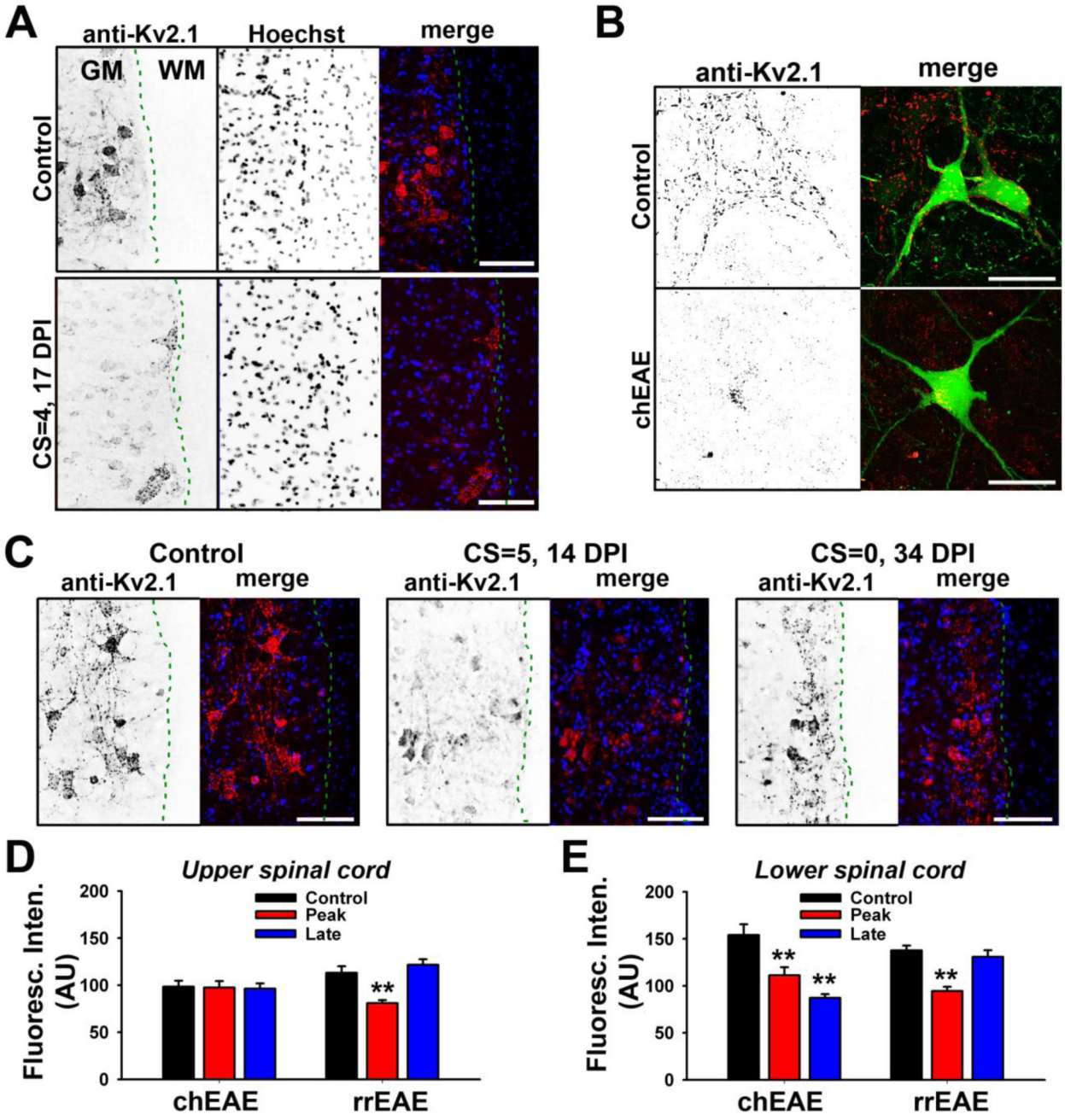

Figure 6. Alterations of somatodendritic Kv2.1 channels in spinal cord motor neurons in chEAE and rrEAE

(**A**) Kv2.1 levels in motor neurons in lower spinal cord of chEAE were significantly reduced. Signals are inverted in single channel images. In merged images, Kv2.1 staining is shown in red and nuclear dye (Hoechst) staining in blue. DPI and CS are provided on the left. Dashed green lines indicate the border between gray matter (GM) and white matter (WM). (**B**) Reduction of somatodendritic Kv2.1 channels in motor neurons in EAE of Thy1:YFP transgenic mice. In merged images, YFP is shown in green and Kv2.1 staining in red. (**C**) Kv2.1 levels in motor neurons of lower spinal cord in rrEAE correlated with clinical signs. The rrEAE mice of control (left), at the peak phase (middle), and at the remitting phase (right), are shown. (**D**) Average Kv2.1 levels in motor neurons of upper spinal cord in

chEAE (Control: 98 ± 6.4 (AU), n = 51; Peak: 97 ± 6.8 (AU), n = 55; Late: 96 ± 5.6 (AU), n = 54) and rrEAE (Control: 113 ± 6.9 (AU), n = 61; Peak: 81 ± 3.3 (AU), n = 63; Late (remitting): 122 ± 5.9 (AU), n = 63). (**E**) Average Kv2.1 levels in the motor neurons of lower spinal cord in chEAE and rrEAE. One-way ANOVA followed by Dunnett's test. ** $p < 0.01$. Scale bars, 150 μm in (**A**) and (**C**); 50 μm in (**B**).

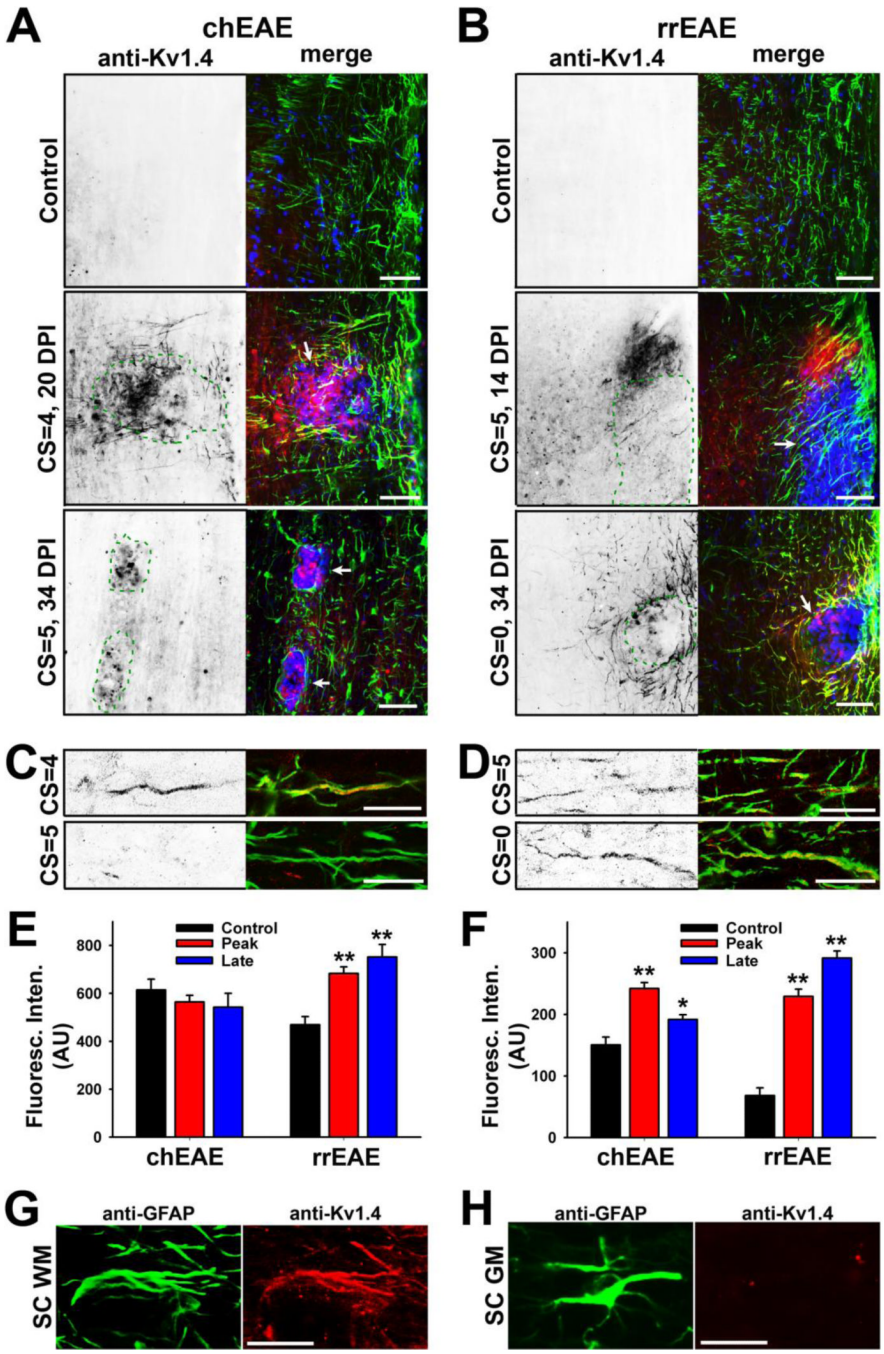

Figure 7. Upregulation of Kv1.4 channels in GFAP-positive cells around EAE lesions

(**A**) Kv1.4 channels markedly increased in spinal cord around lesions in chEAE. In spinal cord white matter, Kv1.4 staining is shown (signals inverted on the left and in red in the merged images on the right) in a control mouse (top), and at the peak (middle) and late (bottom) stages of chEAE. GFAP staining is shown in green and Hoechst staining in blue. DPI and CS are provided on the left. Lesion areas are enclosed with green dashed lines and indicated with white arrows in merged images. (**B**) Kv1.4 channels markedly increased in spinal cord around lesions in rrEAE. The late stage in rrEAE (bottom) is the remitting stage and this mouse had a CS at 4 at the peak stage. (**C**) Confocal images of Kv1.4 colocalizing

with GFAP in the early (top) and late (bottom) chEAE. (**D**) Confocal images of Kv1.4 colocalizing with GFAP at the peak (top) and remitting (bottom) phases of rrEAE. (**E**) Average fluorescence intensities of Kv1.4 in normal and lesion areas. In chEAE: Control, 615 ± 44 (AU), n = 27; Peak, 564 ± 28 (AU), n = 41; Late, 543 ± 58 (AU), n = 18. In rrEAE: Control, 469 ± 34 (AU), n = 28; Peak 683 ± 28 (AU), n = 47; Late (remitting), 752 ± 52 (AU), n = 28. (**F**) Average fluorescence intensities of Kv1.4 along individual processes around the lesions in chEAE and rrEAE mice. Background fluorescence intensity was subtracted for each measurement. One-way ANOVA followed by Dunnett's test. ** $p < 0.01$, * $p < 0.05$. (**G**) High-mag. image of a GFAP-positive (green) astrocyte expressing Kv1.4 (red) in spinal cord white matter during chEAE. (**H**) High-mag. image of a GFAP-positive (green) astrocyte in spinal cord gray matter during chEAE. No Kv1.4 (red) was expressed. Scale bars, 250 μm in (**A**) and (**B**); 25 μm in (**C**) and (**D**); 50 μm in (**G**) and (**H**).

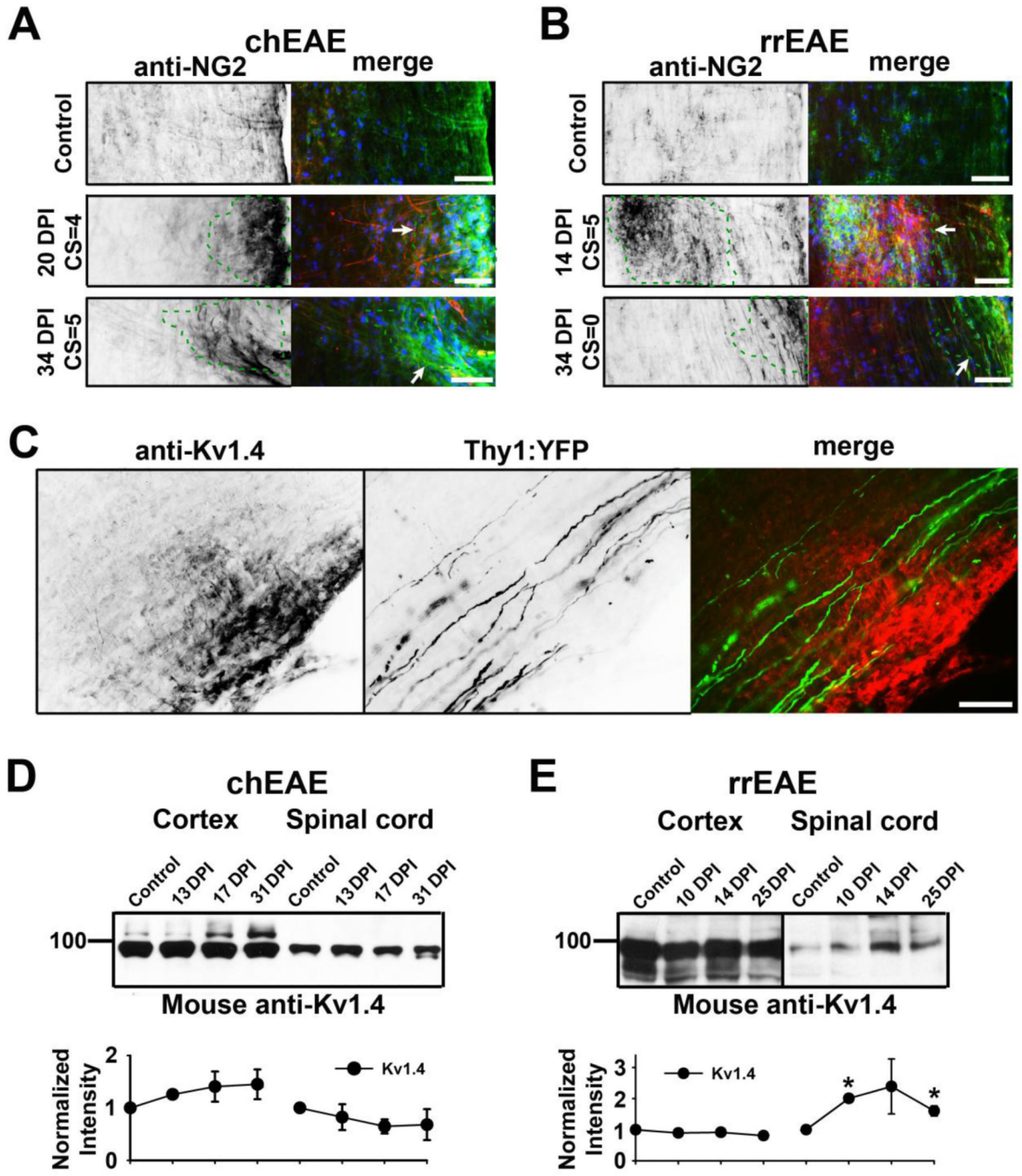

Figure 8. Up-regulated Kv1.4 channels partially colocalized with NG2 but not with YFP-positive axons in Thy1:YFP transgenic mice

(**A**) NG2 staining increased around the lesions in spinal cord white matter of chEAE. NG2 staining signals are inverted on the left image and shown in green in merged images on the right. Kv1.4 staining is shown in red and nuclear dye in blue. Lesion areas are enclosed with green dashed lines and indicated with white arrows in merged images. (**B**) NG2 staining increased around the lesions in spinal cord white matter of rrEAE. (**C**) Up-regulated Kv1.4 around the lesions did not colocalize with YFP-positive axons around chEAE lesions. Kv1.4 staining is in red and YFP in green in the merged image (right). Scale bars, 200 μm. Global expression of Kv1.4 channels revealed by Western blotting of cerebral cortex and spinal

cord at different stages of chEAE (**D**) and rrEAE (**E**). Molecular weight was labeled on the left in kDa. Equal amounts of tissue samples were loaded on the gel. Normalized intensity of protein bands in the Western blotting is shown at the bottom.

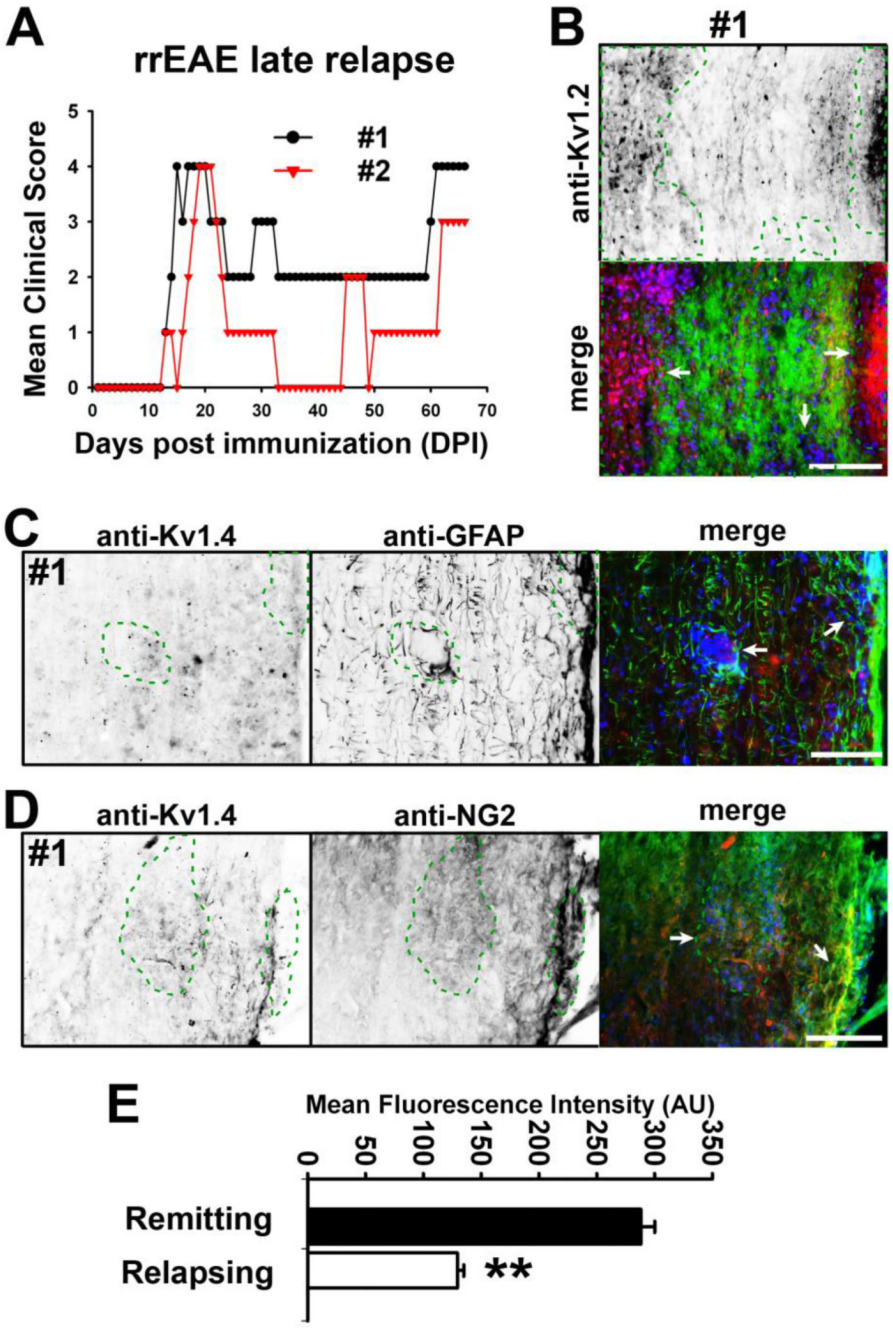

Figure 9. Kv1.4 levels decreased in lesions of spinal cord white matter during the late relapse phase of rrEAE

(**A**) Clinical scores of two rrEAE mice. Both were sacrificed at 66 DPI during the late relapse stage. (**B**) Kv1.2 staining in spinal cord white matter of rrEAE at the relapse stage. Lesion areas are enclosed with green dashed lines and indicated with white arrows. Kv1.2 staining is inverted on the top and in red in the merged image at the bottom. FMG staining is in green and nuclear dye staining in blue. (**C**) Kv1.4 staining decreased in the GFAP positive processes around the lesions. Kv1.4 staining is inverted in the left and in red in the merged image on the right. GFAP staining is inverted in the middle and in green in the merged image on the right. The nuclear dye staining is in blue in the merged image. (**D**) Decreased

Kv1.4 staining only partially colocalized with NG2 staining. NG2 staining is inverted in the middle and in green in the merged image on the right. (E) Statistical results of Kv1.4 staining intensity in the processes around the lesions. Unpaired t-test; **, $p < 0.01$. Scale bars, 250 μm.